Available online at www.sciencedirect.com
ScienceDirect
Ceramics International 37 (2011) 2527–2535
CERAMICS INTERNATIONAL
www.elsevier.com/locate/ceramint

Production and study of in vitro behaviour of monolithic α-tricalcium phosphate based ceramics in the system $Ca_3(PO_4)_2$–Ca_2SiO_4

Isabel M. Martínez [a], Pablo Velásquez [a], Luis Meseguer-Olmo [b], Piedad N. De Aza [a,*]

[a] Instituto de Bioingeniería, Universidad Miguel Hernández, Avda. de la Universidad s/n, 03202-Elche, Alicante, Spain
[b] Unidad de Terapia Celular Hospital Universitario V. Arrixaca-Universidad de Murcia, Spain

Received 25 January 2011; received in revised form 24 March 2011; accepted 31 March 2011
Available online 8 April 2011

Abstract

In this work a new kind of α-tricalcium phosphate (α-$Ca_3(PO_4)_2$) doped with dicalcium silicate (Ca_2SiO_4) ceramic materials, with compositions lying in the field of the $Ca_3(PO_4)_2$ solid solution in the system $Ca_3(PO_4)_2$–Ca_2SiO_4, were obtained. The properties of the sintered ceramics were discussed in detail as well as some in vitro relevant properties for bone repairing. Crystalline α-$Ca_3(PO_4)_2$ solid solution (α-TCPss) was the only phase in the ceramics containing from 1 wt% to 4 wt% of Ca_2SiO_4. The release of ionic Si in simulated body fluid increased with the content of Ca_2SiO_4 and favoured α-$Ca_3(PO_4)_2$ surface transformation. In addition, cell attachment test showed that the α-TCPss supported the mesenchymal stem cells adhesion and spreading, and the cells established close contact with the ceramics after 24 h of culture. According to the results, the investigated α-TCPss ceramics possesses good bioactivity, biocompatibility and mechanical properties, and might be a promising bone implant material.

Keywords: B. Electron microscopy; D. Apatite; E. Biomedical applications; Powder solid-state reaction

1. Introduction

The role of silicon in the formation and maturation of bone has been established since the beginning of the 1970s [1,2]. It is not surprising that bioceramics that incorporate Si into their composition realize higher bioactivity. These include materials with very high Si levels such as Bioglass [3] and Pseudo-wollastonite ($CaSiO_3$) [4,5] as well as CaP-based materials with trace levels of Si doping such as hydroxyapatite (Si-HA) and tricalcium phosphate (Si-TCP) [6,7]. Thus apatite ceramics containing Si are expected to be useful as biodegradable biomaterials to increase the speed of bony regeneration [8,9]. Hydroxyapatite (HA) has been used for many years as bone repairing material. Recently, many attempts to introduce silicon into its network as a way to improve the bioactivity level of the material has been carried out. However, HA is the less soluble of all calcium phosphates and less reactive.

HA is denser and more packed of all calcium phosphates of biological relevance. On the other hand, tricalcium phosphate (TCP) is more soluble and biodegradable than HA, and is expected that Si ions occupying P sites in TCP network are more labile than in the HA network as well.

The hypothesis that supports this work is that TCP with silicon in solid solution should be more reactive than other Si-substituted apatites because of its greater solubility in physiological fluids and lower lattice packing. Thus, this work was aimed to obtain a new kind of Si-containing TCP with compositions lying in the field of tricalcium phosphate solid solution in the system tricalcium phosphate–dicalcium silicate [10,11].

The effect of microstructure (porosity, grain size, phases and silicon content in solid solution), as well as some mechanical properties on the bioactivity and biocompatibility of the TCPss ceramics has been studied, and has been compared its behaviour with pure α-TCP.

2. Materials and methods

2.1. Materials and processing methods

Chemicals used in the synthesis of tricalcium phosphate and dicalcium silicate (C_2S) were calcium hydrogen phosphate

* Corresponding author. Tel.: +34 966 658 485; fax: +34 965222033.
E-mail addresses: i.martinez@umh.es (I.M. Martínez), pvelasquez@umh.es (P. Velásquez), lmeseguer.doc@gmail.com (L. Meseguer-Olmo), piedad@umh.es (P.N. De Aza).

0272-8842/$36.00
doi:10.1016/j.ceramint.2011.03.062

anhydrous ($CaHPO_4 > 98.0$ wt%, Panreac), calcium carbonate ($CaCO_3 > 99.0$ wt%, Fluka) and high-purity silicon oxide ($SiO_2 > 99.7$ wt%, Strem Chemicals). Stoichiometric quantities of the raw powders to obtain tricalcium phosphate and dicalcium silicate were ground in a laboratory mixing miller (MM301-Retsch) by using PSZ-zirconia balls.

TCP was synthesized by solid state reaction from a stoichiometric mixture of calcium hydrogen phosphate anhydrous and calcium carbonate. The dicalcium silicate (C_2S) was obtained by solid state reaction-sintering from a mixture of high-purity silicon oxide and calcium carbonate. In both syntheses the powder were initially calcined at 950 °C for 4 h to decompose $CaCO_3$ following by mixing miller with PSZ-zirconia balls and isopropyl alcohol as suspension media. The powder was then dried and sieved through 30 mesh.

For TCP, the powders were heated in a platinum crucible at 1500 °C for 3 h. Then was liquid-nitrogen quenched by rapid removal from the furnace. For C_2S, the powders were cold isotatically pressed at 200 MPa and heat treated at 1525 °C for 12 h, at a heating rate of 8.3 °C/min followed by cooling rate of 5 °C/min. The reaction-sintering temperature was selected bearing in mind the information provided by the phase equilibrium diagram SiO_2–CaO evaluated and reported by Eriksson et al. [12]. Then the powders thus obtained were ground and characterized by X-ray fluorescence (XRF), X-ray diffraction (XRD) and particle size distribution in powder aqueous suspension (Laser diffraction, Mastersizer S. Malvern).

Stoichiometric quantities of these powders to obtain the compositions of Table 1 were weighed out and thoroughly mixed in a manual agate mortar under acetone. Subsequently, the powders were dried and sieve through 30 mesh. The TCP-C_2S green powders were thereafter isostatically pressed at 200 MPa to form green compacts. In order to optimize the sintering parameters of green compacts of the mix of TCP-C_2S were sintered in air atmosphere at 1500 °C/2 h and then liquid-nitrogen quenched by rapid withdrawal from the furnace. The bars were ground (sieved to <30 mesh) after heat treatment, and then pressed and reheated again. This procedure was repeated three times to homogenize all the compositions. After each thermal treatment the samples were characterized by XRD.

After the homogenization, TCP_{SS} were pressed at 200 MPa and heated up to 1500 °C for 4 h. From this temperature the samples were further cooled inside the furnace down to 1120 °C at a rate of 3.2 °C/min and kept at this temperature for a period of 16 h followed by slow cooling until room temperature by shutting of the current, to obtain dense compacts.

Table 1
Weight % compositions of the ceramic materials.

Symbol	Weight %	
	Ca_2SiO_4	$Ca_3(PO_4)_2$
100-TCP	–	100
99-TCPss	1.0	99.0
98-TCPss	2.0	98.0
97-TCPss	3.0	97.0
96-TCPss	4.0	96.0

2.2. Ceramics characterization.

XRD analyses were carried out (Bruker-AXS D8Advance) to determine the crystalline phases of the different compositions obtained. XRD patterns were recorder from θ to 2θ scans in parafocusing Bragg–Brentano geometry with line focused copper $K_\alpha(\lambda_{Cu,K\alpha1} = 1.54056$ Å) radiation from a conventional sealed tube source. The diffratometer was equipped with a scintillation detector. Scans were taken from 10° to 40° (2θ) in 0.05° steps with counting times of 6 s per step. Owing that X-ray diffraction is sensitive to the crystallite size, the Scherrer formula [13] was used to determine the crystallite size of each material, after instrumental broadening corrections on the assumption that the lattice strain is negligibly small.

$$D = \frac{0.89\lambda}{b\cos\ \theta}$$

where D is the mean crystallite size (nm), 0.89 is the Scherrer constant which depends on the crystal shape, the diffraction line indexes [14], and the dispersion of crystallite sizes of the powder [15], λ is the diffraction wavelength ($\lambda_{Cu,K\alpha1} = 0.15406$ nm), b is the full-width at half-maximum of the peak ($2\theta = 30°$) or integral breadth, after correcting for instrumental peak broadening; and θ is the diffraction angle.

Structural changes were studied by Fourier Transformed Infrared Spectroscopy (FTIR-ThermoNicolet IR200). The FTIR spectra were recorded between 400 cm^{-1} and 1400 cm^{-1}, at 2 cm^{-1} resolution averaging 64 scans. The pellets were prepared by mixing each sample powder with KBr matrix at a level of 1 wt%. The background data were collected for the KBr matrix and subtracted from each spectrum.

The microstructure of sintered samples was studied on specimens polished down to 1 μm diamond paste and chemically etched with diluted acetic acid (1.0%, v/v) for 6 s. Then, they were gently cleaned in an ultrasonic bath with distilled water, dried and palladium coated for Scanning Electron Microscope (SEM-Hitachi S-3500N) observations. Quantitative analyses were made by Wavelength Dispersive X-ray Spectroscopy (WDS) system coupled to the above-described electron microscope using ZAF (atomic number, adsorption, fluorescence) correction software and TCP Bayer standards. Microanalysis data represent the average of ten independent determinations.

Samples for Transmission Electron Microscopy (TEM) were prepared by grinding the sintered samples in alcohol in a pestle and mortar. Drops of the suspension were placed onto carbon coated copper TEM grids of 200 mesh and carbon coated. The powder samples were examined using a Jeol Jem 2010 microscope operated at 200 keV, and 80 cm camera length condition was applied for selected area diffraction patterns (SAD). Electron beam transparent particles were chosen for TEM examination by SAD. High magnification imaging and X-ray energy-dispersive spectrometer (EDS) analysis were also carried out.

Shrinkage of the sintered samples after sintering was determined using the following equation:

$$\text{Shrinkage} = \frac{l_g - l_p}{l_g} \times 100$$

where l_g is the length of green samples and l_p the length of sintered products. Apparent density measurement was performed on each sample by Archimedes' method by immersion in Hg in order to evaluate the degree of densification of the sintered ceramics. The mass of samples was determined using an electric balance and the relative density (RD) is calculated by the following equation:

$$\text{RD} = \frac{\rho_a}{\rho_t} \times 100$$

where ρ_t and ρ_a are theoretical density and apparent density of the samples, respectively.

Knoop hardness was performed on the cross section of the TCPss ceramics using Duramin–Struers microhardness tester. For statistical reasons 21 indentation per sample were used under a load of 200 g for 10 s. By definition, the Knoop hardness (H_k) can be expressed as [16]:

$$H_k = 14229 \frac{L}{d^2}$$

where L denotes the load and d is the long diagonal of the indention. The Knoop hardness tester was also used for the determination of Young's modulus (E). The Young's modulus of TCPss ceramics was evaluated based on the following equation [17]:

$$\frac{b'}{a'} = \frac{b}{a} \alpha \frac{E}{H_k}$$

where b'/a' denotes the indent diagonal after elastic recovery during indention, b/a is the ratio of the Knoop indenter dimensions or geometry (1/7.11); and α is a constant, having a value of 0.45. Twenty one readings were adopted for the average value to evaluate H_k and E.

2.3. SBF in vitro test

In order to estimate the bioactivity of the samples, we used Kokubo and Takadama [18] proposed in 2006 the Tris-buffered simulated body fluid (SBF). Optimized TCPss ceramics bars were cut as discs from bars obtained, and they were 7 mm in diameter and 1.5 mm in thickness. After being ultrasonic washed in isopropyl alcohol and deionized water, they were vertically mounted on a nylon wire in polyethylene falcon test tubes containing 50 ml of SBF at 37 °C and pH = 7.25. The solid/liquid weight ratio was equal to 5×10^{-3}, close to the value used by other authors [19,20]. The SBF was prepared using bottles and flasks, which were all prewashed with a neutral detergent and deionized water. Disc was removed at 1, 2, 3 and 4 weeks of soaking time, gently washed with deionized water, and dried at room temperature.

Sample surfaces and cross-sections, after the exposure to the SBF, were examined by SEM at 20 keV and microanalysis by WDS (Ca, P, and Si). Silicon, calcium and phosphorous ion release profiles were determined for all the samples studied. Additional changes in ionic concentration of the SBF were examined using Inductively Couple Plasma Optical Emission Spectroscopy (ICP-OES). The samples evolution was established by measuring the thickness of the reaction zone and the layer formed in the TCPss ceramics surface by SEM. Thickness data represent the average of ten independent determinations.

2.4. Culture of the bone marrow adult mesenchymal stem cells of human origin

For testing biocompatibility and adhesion of adult mesenchymal stem cells (hMSCs-A) were isolated from bone marrow of three male human volunteers in good physical condition ranging from 27 to 35 years old, obtained through direct aspirations of the iliac crest. The volunteers signed previously an informed consent; also the study was approved by the ethics committee of our institution.

The hMSCs-A were seeded in 75 cm^2 flasks at a density of $5 \times 10^3/cm^2$ and were cultured in α-Minimum Essential Medium (α-MEM) supplemented with 10% fetal bovine serum (FBS) and antibiotics penicillin/streptomycin (100 μg/ml and 100 μg/ml, respectively). The cells were cultured at 37 °C in a 5% CO_2 atmosphere and 95% relative humidity, making a change of medium every 3–4 days. When the culture was confluent, subculture was treated with 0.25% (w/v) Trypsin–EDTA in sterile phosphate-buffered saline (PBS; pH 7.4) for 5 min. For this study only the hMSCs-A at the third passage were employed. In the studies of biocompatibility and adhesion the cells were seeded directly on the materials or were cultured in their presence. Before cell culture studies the ceramics were cleaned applying pressured air and rinsed several times with PBS (pH 7.4). After that, they were dried at 37 °C and finally the pieces were sterilized by plasma gas. Then, the discs of ceramic were introduced in the wells of a 96-well culture plate and cells were seeded onto the ceramics at a density of 1.0×10^4 cells/well. The incubation was carried out at 37 °C, in a 5% CO_2 atmosphere at 95% relative humidity atmosphere. Cell adherence and growth were analysed at 24 h and 7, 15, 21, and 28 days.The surface morphology of samples was analysed by SEM-WDS in order to evaluate the cell growth and adhesion to the ceramics surface. After incubation for 24 h and 7, 15, 21, and 28 days, the samples were removed from the culture well, rinsed with PBS and fixed with 3% glutaraldehyde in 0.1 M cacodylate buffer for 1.5 h at 4 °C. Then they were rinsed and post-fixed in osmium tetroxide for 1 h, before being dehydrated through increasing concentrations of ethanol (30, 50, 70, 90 vol%) with final dehydratation in absolute alcohol. After this, they were dried by the critical-point method and palladium coated and examined by SEM-WDS.

3. Results

3.1. Synthesis of $Ca_3(PO_4)_2$ and Ca_2SiO_4

The X-ray diffraction patterns (Fig. 1A) of the both synthetic TCP and C_2S obtained showed α-TCP and γ-C_2S as the only

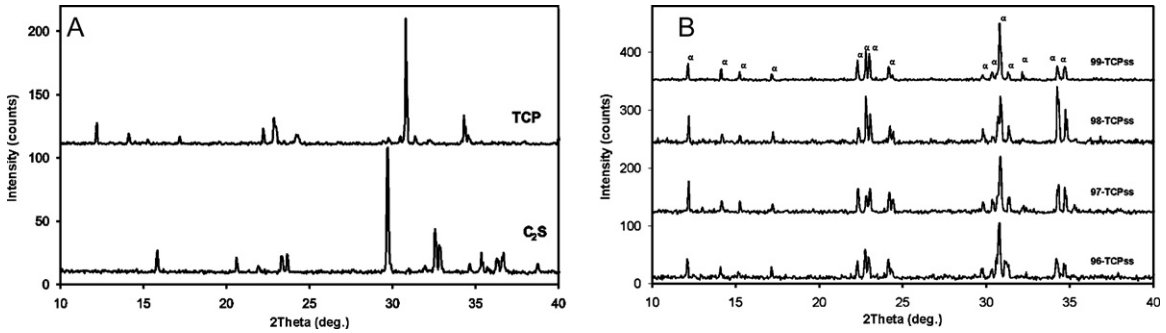

Fig. 1. (A) X-ray diffraction patterns of the synthesized powder: TCP and C_2S, and (B) all the compositions studied.

phase being present, respectively. Both compounds were ground to an average particle size of 20 μm and 15 μm respectively. The results of chemical analysis by XRF, for both materials, are shown in Table 2.

3.2. TCPss ceramics

The XRD data corresponding to the TCPss samples are shown in Fig. 1B. In all samples the phase detected were metastable α-TCP (high temperature polymorph of TCP) regardless of the addition of C_2S. The $\beta \rightarrow \alpha$ polymorphic transition in TCP with high purity takes place at 1125 °C [21–24]. However, the presence of Si in solid solution in TCP shifts the transition temperature to lower temperatures. This solid solution explains the presence of the α-polymorph at room temperature. Based on XRD patterns, the grain size of TCPss compositions studied are given in Table 3. The grain size decreased with the increasing Si content from 207 nm to 85 nm.

Table 2
Results of the X-ray fluorescence chemical analysis of the TCP and C_2S synthetic powders.

Chemical analysis (wt%)	$Ca_3(PO_4)_2$	Ca_2SiO_4
CaO	54.22	44.62
SiO_2	ND	55.28
P_2O_5	45.74	ND
MgO	0.33	ND
Na_2O	0.10	ND
K_2O	0.008	ND
Fe_2O_3	0.037	ND
TiO_2	0.012	ND
SrO	0.004	ND

ND: non detected (below the limit of determination of the analytical method).

This finding agrees well with other data of Si-containing-TCP obtained by other methods reported in the literature [25].

For a comprehensive microstructural characterization of the materials, microstructural parameters such as porosity density and shrinkage and amount of silicon in solid solution in TCP have been established (Table 3). The tendency for the density was to increase with the increasing amounts of shrinkage; in this way it was possible to observe that the sample that shows highest shrinkage, corresponding to that of 96-TCPss, showed also the highest density and high silicon content in solid solution.

The Knoop hardness (H_k), Vicker hardness (H_v) and Young's modulus (E) of α-TCPss ceramics are shown in Table 4. The variation of the H_k, H_v and E of α-TCPss ceramics is similar to that of the density results. Like the results of the relative density, the Knoop, Vicker hardness and Young's modulus increase with the content of silicon in solid solution, although there are no bigger differences between them.

Fig. 2 compares FTIR of pure α-TCP (Fig. 2A) with the compositions TCPss (Fig. 2B–E). All spectra present strong similarities, they exhibit intense bands attributed to PO_4^{3-} groups. The bands in the range 1125–1070 cm^{-1} are assigned to the components of the triply degenerated asymmetric terminal P–O stretching mode (ν_3). The symmetric terminal P–O stretching bands, non-degenerated, appear at 970 cm^{-1} (ν_1). Between 550 cm^{-1} and 620 cm^{-1} appear the bands corresponding to the triply degenerated ν_4, corresponding to the symmetric bending vibrations of O–P–O. The bands at 420 cm^{-1} and 460 cm^{-1} are attributed to the doubly degenerated O–P–O bending mode (ν_2) [26]. The spectra of TCP_{SS} materials also show a weak shoulder at 1109 cm^{-1} due to the Si–O–Si asymmetric stretching bands, indicating the presence of silicate groups. This band is not observed in α-TCP

Table 3
Physical characteristic of the ceramics.

	Crystalline phases	Grain size (nm)	Si (wt%)	Porosity (%)	Density (g cm^{-3})	RD (%)	Shrinkage (%)
100-TCP	α-TCP	207	–	28	2.21	77.27	17.7 ± 0.5
99-TCPss	α-TCPss	192	0.23 ± 0.01	27	2.22	77.60	17.8 ± 0.5
98-TCPss	α-TCPss	159	0.26 ± 0.01	21	2.33	81.47	17.9 ± 0.5
97-TCPss	α-TCPss	129	0.29 ± 0.01	16	2.38	83.21	18.3 ± 0.5
96-TCPss	α-TCPss	85	0.30 ± 0.01	14	2.46	86.01	18.4 ± 0.5

Theoretical density of α-TCP = 2.86 g/cm^3.

Table 4
Mechanical properties of the samples.

	H_k	H_v	E (GPa)
100-TCP	0.26 ± 0.25	0.61 ± 0.5	24.3 ± 0.5
99-TCPss	0.27 ± 0.20	0.61 ± 0.5	24.3 ± 0.5
98-TCPss	0.28 ± 0.10	0.62 ± 0.5	24.4 ± 0.5
97-TCPss	0.32 ± 0.70	0.63 ± 0.5	24.6 ± 0.5
96-TCPss	0.33 ± 0.09	0.67 ± 0.5	25.5 ± 0.5

spectrum. Unfortunately, the main bands corresponding to the silicate group, due to the SiO_4^{4-} tetrahedra overlaps with the same type of vibrations in the PO_4^{3-} tetrahedra, consequently they cannot be distinguished. Moreover, the effect of silicon in solid solution causes a substantial narrowing of the P-O stretch peak and a shift in its position to upper wavenumbers [27].

Prior to exposure to cell culture medium the finished surfaces without polishing of the bioceramic samples obtained were observed by SEM. This revealed a rough surface and a homogeneous microstructure. Fig. 3 shows a SEM micrograph of the 97-TCPss ceramic as a representative of all compositions. No significant microstructural features can be observed except closed pores of average size ≈10–15 μm. The total porosity of the samples was measured using twenty SEM micrographs per composition. From the microphotograph it can be said that the ceramic only present one phase, with C_2S in solid solution, as detected by WDS. This finding is in good agreement with the XRD results where only α-TCPss phase is detected. WDS analysis (Table 3) shows the composition of the TCPss studied in terms of wt % of Si.

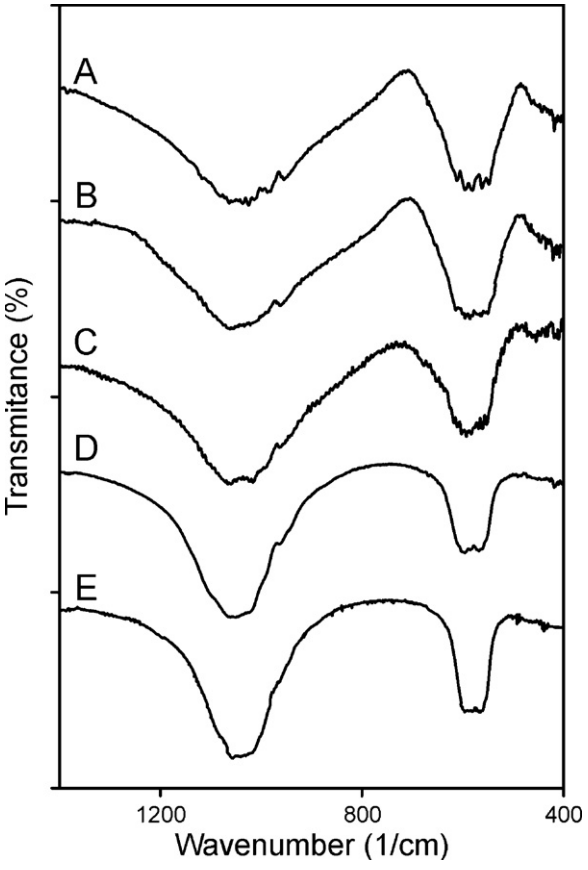

Fig. 2. FTIR spectra for the materials (A) α-TCP, (B) 99-TCPss, (C) 98-TCPss, (D)97-TCPss, and (E) 96-TCPss.

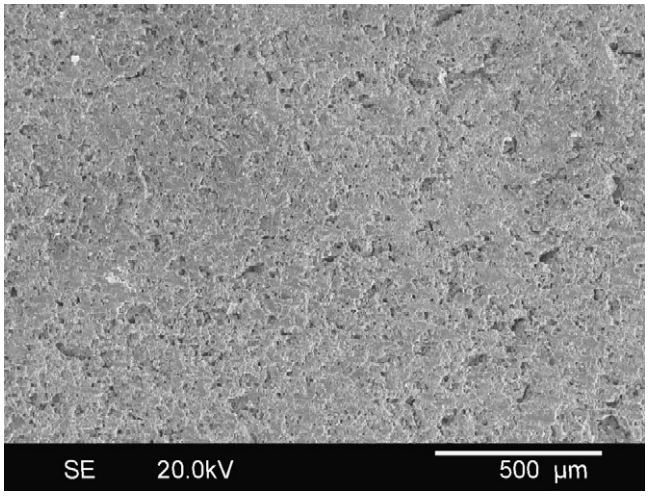

Fig. 3. SEM micrograph of 97-TCPss ceramic.

Fig. 4 shows a TEM image of a single powder particle approximately 30 nm in large for a composition 97-TCPss ceramic as a representative of all compositions. This particle consists of five grains easily identifiable due to lattice matching within the image. Variations in the gray scale across the picture are likely due to changes in thickness. The main orientations of the lattice planes are sketched in Fig. 4B. The largest grain, found at the top of the particle was chosen for further evaluation. Fig. 4C shows the upper region at a higher magnification where the lattice spacing was measured to be 0.290 nm [28].

Fig. 4D is a selected area diffraction pattern from the same grain. The lattice spacings associated with the spots in this pattern were determined using the monoclinic crystallographic structure of P21/a as identified by X-ray diffraction (Fig. 1B) JCPDS n°-29-0359. When the specimen was appropriately oriented, the SAD often displayed (1 3 2), (0 3 4) and (2 9 0) spots corresponding to the 0.3882, 0.2909, 0.2619 nm lattice spacing, indicating on the preferential orientation of the TCPss crystals in the layer. Fig. 4E displays the measured values of the lattice spacings obtained from the SAD pattern (Fig. 4D) and ASTM data from α-TCP (JCPDS n°-29-0359).

3.3. SBF in vitro test

The surface morphologies of the ceramics after soaking in SBF for 1 and 2 weeks are shown in Fig. 5A and B respectively. After immersion, the material surface was covered by a layer of small agglomerates of globular particles. This morphology does no further change with soaking time although the size of the aggregates increases, and the surface was fully covered at 2 weeks of immersion as can be clearly seen in Fig. 5B. Fine small agglomerate particles were observed inside the pores formed on the surface of the samples (Fig. 6A). These small agglomerate particles were determined to be bone-like apatite

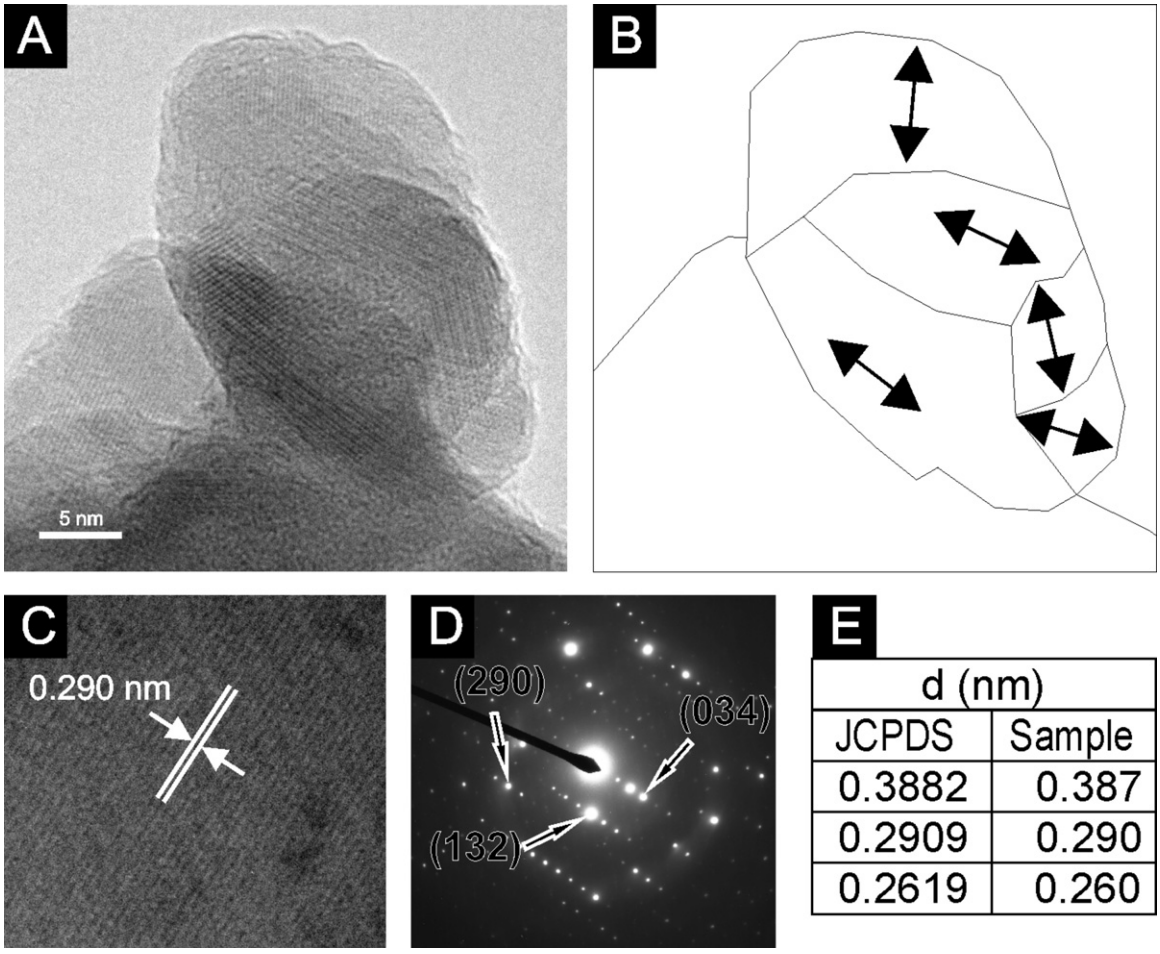

d (nm)	
JCPDS	Sample
0.3882	0.387
0.2909	0.290
0.2619	0.260

Fig. 4. TEM micrographs of sample 97-TCPss ceramic (A)TEM, (B) regions of different crystal orientation, (C) HRTEM, (D) SAD, and (E) lattice spacing of the 97-TCPss phase, taken from SAD of (D) and ASTM data.

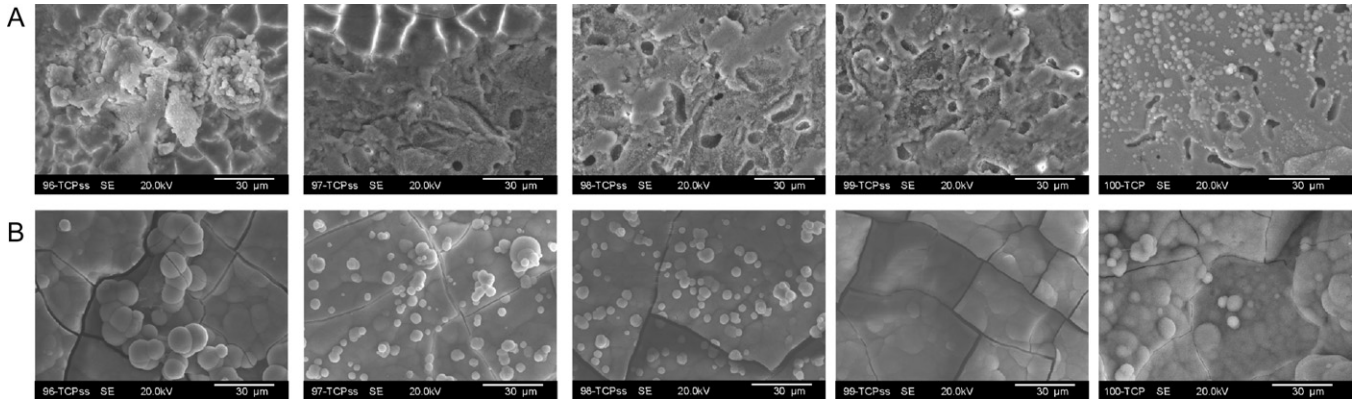

Fig. 5. SEM images of the bioceramics after immersion in SBF for (A) 1 week, and (B) 2 weeks.

(Fig. 6B) although from SEM-WDS microanalysis the Ca/P ratio of the apatite-like layer was in average 2.3, higher than that in HA. This fact suggest that carbonate hydroxyapatite (CHA) is forming on the surface according to the results reported by other authors [29–31].

Table 5 shows the relationships between soaking time and thickness of layers developed on the surface of the ceramics. It is clear to see from Table 5 that two layers were observed on the surface of the ceramic. A top layer, in contact to SBF, of (39.70 ± 0.5 μm) of thickness and rich in Ca and P as detected by WDS analysis; the Ca/P ratio was 2.4 suggesting the formation of CHA. And an intermediate layer of (40.10 ± 0.5 m) of thickness due the dissolution and pseudomorphic transformation of TCPss in HA-like as well as the filling of the porous, with a Ca/P ratio of 1.68, which was close to that of the stoichiometric HA (1.67). Also the layer present some traces of

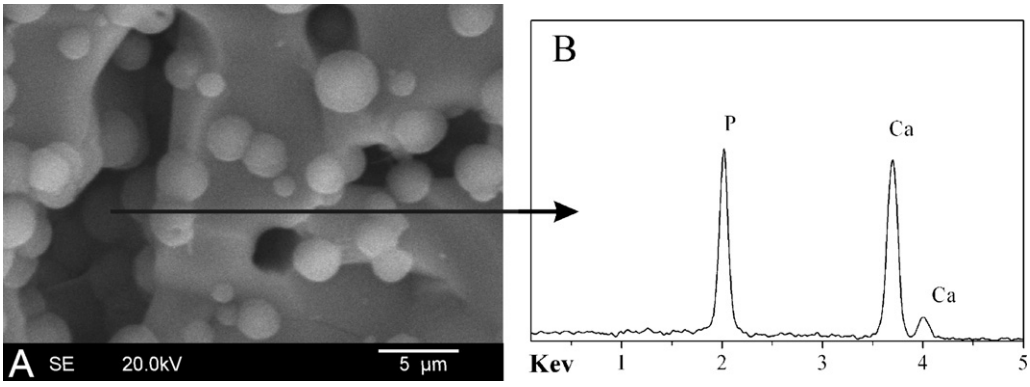

Fig. 6. SEM view of a pore in the 97-TCPss ceramic after immersion in SBF for 1 week being filled by CHA and WDS analyses.

Table 5
Thickness of the Ca/P layer on the surface of each ceramic studied after 4 weeks of soaking in SBF.

Time/thickness (μm)	100-TCP	99-TCPss	98-TCPss	97-TCPss	96-TCPss
Outer layer (±0.5)					
4 weeks	34.50	35.43	38.50	37	39.70
Inner layer (±0.5)					
4 weeks	0	0	34	35	40.10

silicon, which could be produced by the diffusing rate of the silicon ions to the surface. The α-TCPss ceramics release Si ions during immersion in SBF and their amount increased with C_2S content, as shown in Fig. 7. Similar effects were observed in samples with 97 and 98-TCPss. Otherwise the samples 100-TCP and 99 wt%TCP does not present the intermediate layer.

3.4. Cell test

Fig. 8 shows the morphology of hMSCs-A adhering and spreading on α-TCPss ceramics after incubation for 24 h and 28 days. In the first 24 h of culture (Fig. 8A) the ceramics exhibited a granular layer that covers part of the surface with spiculas and small nodules that correspond to a Ca–P deposit according to microanalysis by SEM-WDS observations. The adhesion was enhanced by means of multiple cytoplasmic digitations that spread across the surface of the material, increasing the contact area with the surface material. At this period the cells in all the ceramics studied presented a similar morphology showing some cells adhering either individually or in small groups dispersed across the surface of the material. After 28 days of incubation (Fig. 8B), the cells spread and presented a close contact with the materials, and the philopodia projected progressively. Also abundant extra-cellular matrix was also observed at this time. The intercellular gaps were occupied by abundant fibrillar material, with deposits of mineral forming an extra-cellular matrix. To determine the nature of the nodules, microanalysis by WDS was carried out. This analysis proved that it was a calcium phosphate-based material. It is worth noting that this WDS spectrum is different to that of the material surface, which showed peaks corresponding to Si, Ca and P.

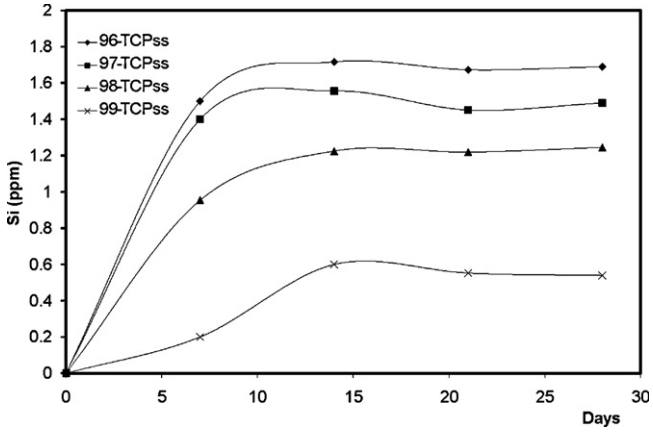

Fig. 7. Si release (ppm) profile of the α-TCPss in SBF.

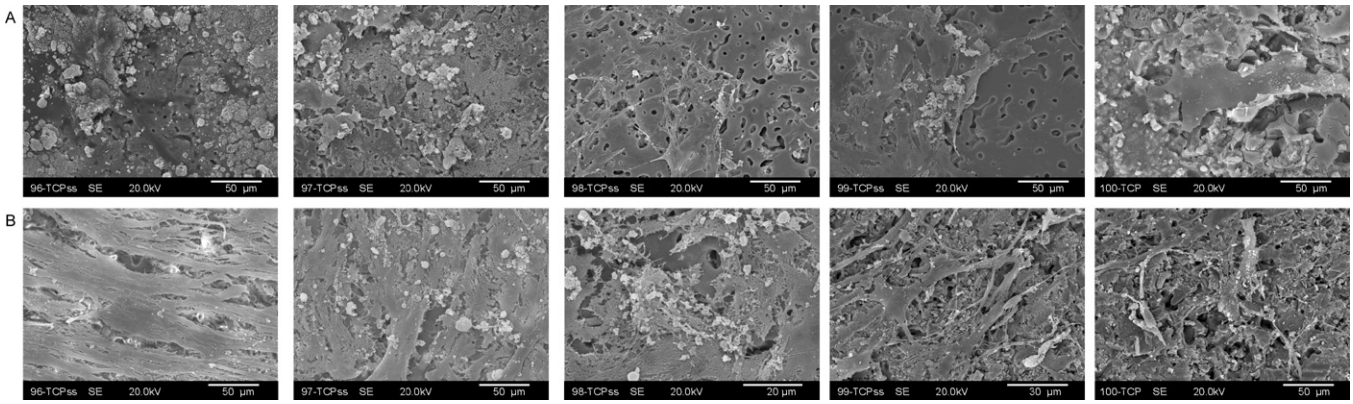

Fig. 8. SEM images of the morphology of hMSCs-A growing on the bioceramics after (A) 24 h and (B) 28 days.

4. Discussion

The aforementioned experimental results are of value from two different points of view: (a) α-TCP was successfully prepared by a new single-stage technique, and (b) α-TCPss appeared to be easily ''mineralizable'' in vitro.

The first conclusion of this work showed that small level of C_2S substitution had a strong effect on the thermal stability of the α-TCP. The substitution of silicate ion into α-TCP clearly helps stabilise the high temperature α-polymorph, which must normally be quenched rapidly to room temperature from temperatures above 1125 °C [21–24]. This may enable large quantities of the α-polymorph to be prepared more easily, removing the need such rapid quenching. The α-TCP remains metastable at room temperature and XRD data has proved that there was only α polymorph present in the TCP_{SS} samples. Furthermore, SEM micrographs and WDS analysis have also shown that only one homogeneous phase is present in all the compositions studied. The TEM observations of relatively large volumes of uniform crystalline material within a single powder particle suggest that Si may diffuse during firing to effect a uniform distribution.

As compared the α-TCPss ceramics, revealed the improvement mechanical properties with the silicon content in solid solution as well as densification. Previous studies have shown that the mechanical strengths of the sintered ceramics were correlated with the densification as well as the grain size and mechanical properties [32–35]. In our study, the average relative density obtained for α-TCPss ceramic was only 82.1%, which suggests that a further improvement of the mechanical properties might be possible by controlling microstructure according to conventional processing methods in advance ceramics. The advantage of α-TCPss materials is to combine biological activity, control microstructure and enough mechanical stability.

There are similarities between the results of the current study and those available in the literature, that may be explained by improved mineralization ability of Si-TCP, if compared with the chemically pure TCP. Our results pointed to a more favourable mineralization of α-TCPss, which again correlates well with other Si-CaP previous finding by other researchers. For example, for silicon containing TCP, the time required to form a surface apatite layer on Si-TCP in SBF decreased with increasing silicate ion substitution [4,8].

Several studies [36,37] have shown that surface roughness is an important parameter in basic cell biological responses, improving cell attachment and proliferation. hMSC-A demostrated significantly higher levels of cell attachment on rough sandblasted surfaces with irregular morphologies than on smooth surfaces [37]. The ceramic samples studied in the present work exhibited a rough surface morphology, as shown in Fig. 3. Thus, the surface properties of the material can help to promote hMSC-A cell attachment.

Additionally, it was observed that after seeding cells on the ceramics, the cells underwent their morphological changes to stabilize the cell-biomaterial interface, and the cells spread and established close contacts with the ceramics, adapting a flattened morphology and showing numerous filopodia anchoring the cells to the bioactive ceramics after 24 h. This behaviour indicate that all the α-TCPss ceramics support the cell adhesion and it was more evident in the 96-TCPss ceramic. Also, the present results verify that features such as composition and roughness can modulate cells responses in vitro.

5. Conclusions

A novel α-TCPss ceramics can be fabricated by sintering TCP-C_2S green compacts. Small level of C_2S substitution in TCP has a strong effect on the thermal stability of the α-TCP. C_2S addition lowers the temperature of phase transition from β-TCP to α-TCP. This has an immediate advantage in that the quenching conditions are not as critical for the production of α-TCPss compositions compared to silicate-free α-TCP.

The mechanical properties of the ceramics are dependent on the amount of silicon in TCPss. The in vitro studies show that α-TCPss ceramics induced formation of a CHA layer in SBF within 1 week and supported osteogenic cells adhesion and spreading. Because of its characteristics, the α-TCPss ceramic might be a promising candidate as implant materials.

Acknowledgements

Part of this work was supported by CICYT under project no. MAT2006-12749-C02-02.

References

[1] E.M. Carlisle, Silicon: a posible factor in bone calcification, Science 167 (1970) 279–280.
[2] E.M. Carlisle, Silicon: an essential element for the chick, Science 178 (1972) 619–621.
[3] L. Hench, Bioceramics: from concept to clinic, J. Am. Ceram. Soc. 74 (1991) 1487–1510.
[4] R.G. Carrodeguas, A.H. De Aza, J. Jiménez, P.N. De Aza, P. Pena, A. Lopez-Bravo, S. De Aza, Preparation and in vitro characterization of wollastonite doped tricalcium phosphate ceramics, Key Eng. Mater. 361–363 (2008) 237–240.
[5] P.N. De Aza, A.H. De Aza, S. De Aza, Crystalline bioceramic materials, Bol. Soc. Esp. Ceram. Vidr. 44 (3) (2005) 135–145.
[6] J.W. Reid, L. Tuc, M. Sayer, K. Fargo, J.A. Hendry, Synthesis and characterization of single-phase silicon-substituted α-tricalcium phosphate, Biomaterials 27 (2006) 2916–2925.
[7] S.M. Best, A.E. Porter, E.S. Thian, J. Huang, Bioceramics: past, present and for the future, J. Eur. Ceram. Soc. 28 (2008) 1319–1327.
[8] A.E. Porter, N. Patel, J.N. Skepper, S.M. Best, W. Bonfield, Comparison of *in vivo* dissolution processes in hydroxyapatite and silicon-substituted hydroxyapatite bioceramics, Biomaterials 24 (2003) 4609–4620.
[9] A.M. Minarelli-Gaspar, S. Saska, R.G. Carrodeguas, A.H. De Aza, P. Pena, P.N. De Aza, S. De Aza, Biological response to wollastonite doped α-tricalcium phosphate implants in hard and soft tissues in rats, Key Eng. Mater. 396–398 (2009) 7–10.
[10] W. Fix, H. Heymann, R. Heinke, Subsolidus relations in the system $2CaO{\cdot}SiO_2$–$3CaO{\cdot}P_2O_5$, J. Am. Ceram. Soc. 52 (6) (1969) 346–347.
[11] I.M. Martinez, P.A. Velasquez, P.N. De Aza, Synthesis and stability of α-tricalcium phosphate doped with dicalcium silicate in the system $Ca_3(PO_4)_2$–Ca_2SiO_4, Mater. Charact. 61 (2010) 761–767.
[12] G. Eriksson, P. Gu, M. Blander, A.D. Pelton, Critical evaluation and optimisation of the thermodynamic properties and phase diagrams of the MnO–SiO_2 and CaO–SiO_2 systems, Can. Metall. Q. 33 (1994) 13–21.
[13] H. Klug, L. Alexander (Eds.), X-Ray Diffraction Procedures, Wiley, New York, 1962, p. p. 125.
[14] C.G. Shull, The determination of X-ray diffraction line widths, Phys. Rev. 70 (1946) 679–684.
[15] R. Pielaszek, Diffraction studies of microstructure of nanocrystals exposed to high pressure, Ph.D. Thesis, Warsaw University, Dept. Physics, Warsaw, Poland, 2003.
[16] G.F.V. Voort, G.M. Lucas, Microindentation hardness testing, Adv. Mater. Process 5 (1998) 21–25.
[17] A. Slosarczyk, J.J. Bialoskorski, Hardness and fracture toughness of dense calcium phosphate based materials, J. Mater. Sci.: Mater. Med. 9 (1998) 103–108.
[18] T. Kokubo, H. Takadama, How useful is SBF in predicting *in vivo* bone activity? Biomaterials 27 (2006) 2907–2915.
[19] T. Kokubo, Novel bioactive materials, An. Quim. 93 (1) (1997) 49–55.
[20] I.J. Izquierdo-Barba, A. Salinas, M. Vallet-Regi, Effect of the continuous solution exchange on the in vitro reactivity of a CaO–SiO_2 sol–gel glass, J. Biomed. Mater. Res. 51 (2) (2000) 191–199.
[21] M.J. Buerger, The role of temperature in mineralogy, Am. Mineral. 33 (3–4) (1948) 101–121.
[22] M.J. Buerger, in: R. Smoluchowski, J.E. Meyer, W.A. Weyl (Eds.), Crystallographic Aspects of Phase Transformations in Phase Transformations in Solids, John Wiley and Sons Inc., New York, 1951, pp. 183–211.
[23] J.H. Welch, W. Gutt, High-temperature studies of the system calcium oxide–phosphorus pentoxide, J. Chem. Soc. (1961) 4442–4444.
[24] R.G. Carrodeguas, A.H. De Aza, X. Turrillas, P. Pena, S. De Aza, New approach to the $\beta \rightarrow \alpha$ polimorphic transformation in magnesium-substituted tricalcium phosphate and its practical implications, J. Am. Ceram. Soc. 91 (4) (2008) 1281–1286.
[25] M. Kamitakahara, T. Kurauchi, M. Tanihara, K. Ioku, C. Ohtsuki, Synthesis of Si-containing tricalcium phosphate and its sintering behaviour, Key Eng. Mater. 361–363 (2008) 59–62.
[26] A. Slosarczyk, C. Paluszkiewicz, M. Gawlicki, Z Paszkiewicz, The FTIR spectroscopy and QXRD studies of calcium phosphate based materials produced from the powder precursors with different Ca/P ratios, Ceram. Int. 23 (1997) 297–304.
[27] C.Q. Ning, J. Mehta, A. El-Ghannam, Effects of silica on the bioactivity of calcium phosphate composites in vitro, J. Mater. Sci.: Mater. Med. 16 (2005) 355–360.
[28] M. Matthew, L.W. Shroeder, B. Dickens, WE Brown, The crystal structure of α-$Ca_3(PO_4)_2$, Acta Crystallogr. B33 (1977) 1325–1333.
[29] P.N. De Aza, Z. Luklinska, M. Anseau, F. Guitian, S. De Aza, Electron microscopy of interfaces in a wollastonite-tricalcium phosphate bioeutectic material, J. Microsc.-Oxford 189 (2) (1998) 145–153.
[30] A.M. Minarelli-Gaspar, S. Saska, L.R. da Cunha, P.D.A. Bolini, R.G. Carrodeguas, A.H. De Aza, P. Pena, P.N. De Aza, S. De Aza, Comparison of the biological behaviour of wollastonite bioceramics prepared from synthetic and natural precursors, Key Eng. Mater. 361–363 (2008) 1083–1086.
[31] Z.B. Luklinska, W. Bonfield, Morphology and ultrastructure of the interface between hydroxyapatite–polyhydroxybutyrate composite implant and bone, J. Mater. Sci.: Mater. Med. 8 (1997) 379–383.
[32] J.S. Moya, P. Pena, S. De Aza, Transformation toughening in composites containing dicalcium silicate, J. Am. Ceram. Soc. 68 (1985) C259–C262.
[33] J.L. Shi, Thermodynamics and densification kinetics in solid-state sintering of ceramics, J. Mater. Res. 14 (1999) 1398–1408.
[34] R.W. Rice, Grain size and porosity dependence of ceramic fracture energy and toughness at 22 °C, J. Mater. Sci. 31 (1996) 1969–1983.
[35] C.X. Wang, X. Zhou, M. Wang, Influence of sintering temperatures on hardness and Young's modulus of tricalcium phosphate bioceramic by nanoindentation technique, Mater. Charact. 52 (2004) 301–307.
[36] J.Y. Martin, Z. Schwartz, T.W. Hummert, D.M. Schraub, J. Simpson, J Lankford, et al., Effect of titanium surface-roughness on proliferation, differentiation, and protein-synthesis of human osteoblast-like cells (MG63), J. Biomed. Mater. Res. 29 (1995) 389–401.
[37] K.T. Bowers, J.C. Keller, B.A. Randolph, D.G. Wick, C.M. Michaels, Optimization of surface micromorphology for enhanced osteoblast responses in vitro, Int. J. Oral Maxillofac. Implants 7 (1992) 302–310.